



Model Test on Uplift Capacity of Short Pile Foundation on Clay Foundation

Weizhou Xu*, Bo Wang, Zengjun An

Economic Research Institute, State Grid Jiangsu Electric Power Company, Nanjing Jiangsu
210008, China

Email: 1432515418@qq.com (Weizhou Xu);
2875893494@qq.com (Bo Wang);
1312027119@qq.com (Zengjun An)

Abstract. Piles with a small slenderness ratio (short piles) have the characteristics of high rigidity and small deformation, which meets the requirements for promoting mechanized construction. This paper designs short pile models with three slenderness ratio ratios to test the uplift capacity characteristics of short piles on clay foundations. The load-deformation characteristics and development laws of short pile foundations under different slenderness ratios are studied. The results indicate that the short pile foundation on the clay foundation showed a composite shear failure mode. The ultimate uplift capacity of short pile foundation is positively correlated with the pile slenderness ratio. The theoretical calculation value of short pile foundation is relatively conservative. In the design of short pile foundations, the slenderness ratio of the pile must be controlled to balance economy and performance.

Keywords: short pile foundation; model test; uplift capacity; clay; slenderness ratio

1 Introduction

The short pile foundation of power transmission lines in China is generally designed according to DL/T5486-2020 [1], which has the characteristics of high rigidity and small deformation and is conducive to mechanized construction [2-8]. Transmission tower structure foundations are often subjected to uplift loads [9]. Therefore, it is important to understand the uplift capacity of short pile foundations [10-11]. BRAJA [12] proposed a preliminary general procedure for estimating the ultimate pullout capacity of foundations in clays, based on the results of laboratory model tests on rectangular foundations in saturated clays. Dash et al. [13] studied the effects of multiple parameters on the uplift capacity of piles, including different sand types, embedment depth, and slenderness ratio. Research has shown that compressive loads on piles can reduce their net tensile bearing capacity. In addition, the type of soil affects the stress and bearing capacity characteristics of pile foundations [14]. Therefore, Reddy et al. [15]

inhomogeneous clays and confirmed that the theoretical values are higher than the actual values. Usually, using short pile foundations in the design of transmission towers can improve the efficiency of foundation excavation and reduce the safety risks of construction, which meets the requirements of promoting mechanized construction. However, existing studies have not agreed on the variation of the ultimate bearing capacity of short piles in clay [16-21]. Therefore, the bearing capacity and theoretical calculation of short pile foundations on clay foundations must be studied urgently.

In summary, this paper carried out a model test on the uplift capacity of short pile foundations on clay foundations, studied the load-deformation characteristics and development laws of short pile foundations under different slenderness ratios, and explored the design theory of the uplift capacity of short piles in clay foundations. The research results can provide insights into the design of short pile foundations for transmission lines on clay.

2 Experimental Details

2.1 Dimensions of Model Pile

The pile model designed for this paper is made of organic glass with a diameter D of 35mm. A total of three groups of specimens (i.e., BDZ1, BDZ2, and BDZ3) are manufactured, with pile lengths L of 245 mm, 350 mm, and 525 mm, corresponding to three different slenderness ratios, i.e., $L/D=7$, 10, and 15. In order to study the strain development characteristics and laws of the model pile during loading, the resistance strain gauges are arranged at typical locations of the pile body to test the strain changes at different parts during loading. Therefore, notches are set on both sides of the pile body to facilitate the pasting of strain gauges and lead-out wires, and a hole is opened on the top of the pile to facilitate loading. The strain gauges are pasted at the quarter of the pile body, with three locations, and arranged symmetrically along both sides of the model pile. The specific pasting positions are shown in Fig 1. The strain gauge model is BE120-5AA, which is 10 mm \times 4 mm. At the same time, a vertical displacement meter is set to measure the vertical displacement of the short pile top during the uplift loading process to obtain the load-displacement curve of the short pile.

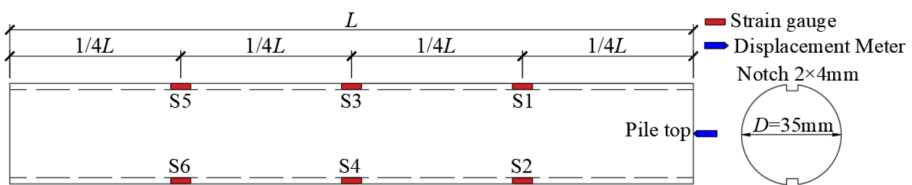


Fig. 1. Size of model pile and measurement point layout

2.2 Soil for Model Testing

The water ratio of typical soft plastic clay is determined by screening, trial mixing, and testing. Then, soil for the model test is prepared. The soil parameters of the foundation soil for the short pile foundation test are obtained according to the geotechnical test and are shown in Table 1.

Table 1. Parameters of test soil

Parameter	Unit	value
Moisture content	%	21.1
Density	g/cm ³	2.02
Dry density	g/cm ³	1.67
Porosity ratio	/	0.590
Saturation	%	98
Plasticity index	/	18.2
Liquidity Index	/	0.01
Compression factor	MPa ⁻¹	0.21
Compression modulus	MPa	7.57
Cohesive force	kPa	58.8
Internal friction angle	°	16.6

2.3 Test Model

After the strain gauge is pasted on the notches of the model pile, AB glue and a layer of proportional fine sand are evenly applied on the surface and groove of the pile. This way can not only protect the strain gauge from being scratched by fine stones or other debris in the soil but also better simulate the friction between the pile body and the soil to obtain accurate load-strain development of the model pile under graded horizontal loads, as shown in Fig 2(a). The model soil in the soil box is backfilled and compacted in layers. Model piles of various sizes are buried in the model soil. When the test model is made, it is sealed and locally loaded for more than 4 weeks to ensure that the test clay is fully consolidated, as shown in Fig 2(b).



Fig. 2. Test model: (a) Model pile; (b) Test model

2.4 Loading Protocol

A self-designed multi-point loading test device, which consists of a loading lever, reaction beam, and lever support, is used for loading in this test, as shown in Fig. 3. The hinge support of the loading lever is installed on the upper side of the reaction frame. One end of the lever is connected to the pile foundation model through a steel strand, and a mass is hung on the other end to achieve multi-point loading. According to relevant specifications [1], this project adopts the rapidly maintained load method. First, the theoretical value of the ultimate capacity of each pile foundation model is calculated. Then, the pile foundation model is subjected to graded equal loading, with the value being 1/8~1/5 of the estimated ultimate capacity. In addition, the weight of the loading lever and the basket are considered. Therefore, the first level load is 2 to 3 times the graded load. After each load level is stable, the strain gauge data at different parts of the pile body are tested and recorded.

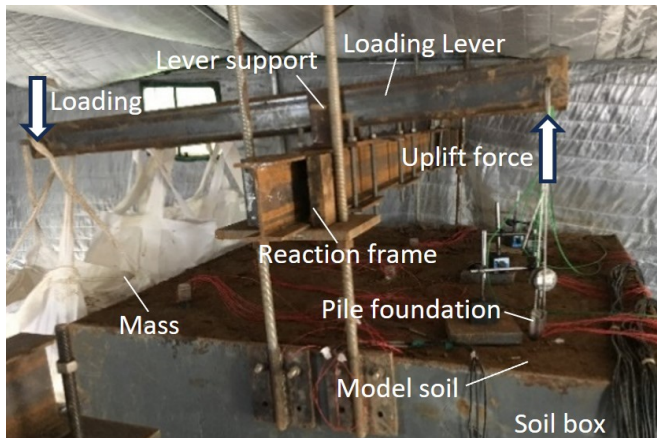


Fig. 3. Test set up

3 Test Results

3.1 BDZ1

For the steep-rising load-displacement curve, the bearing capacity is the load value corresponding to the starting point where the obvious steep rise occurs [1]. Fig. 4 shows the load-displacement curve of model pile BDZ1. It can be observed that in the early stage of loading, the uplift displacement increases slowly. With the gradual increase of the uplift load, the growth amplitude of the uplift displacement increases rapidly. Therefore, the uplift capacity of the short pile foundation BDZ1 on clay foundation is determined by the test to be 0.281 kN, and the uplift displacement is 1.39 mm. When the load reaches 0.423kN, the pile BDZ1 is pulled out as a whole. It can be seen that during the uplift loading process of the short pile foundation BDZ1 on the clay foundation, obvious cracks are formed in the soil around the pile. An oblique fracture surface is

formed in the soil, and the conical soil adheres to the pile. This is because the shear strength and internal friction angle of clay are relatively small, and the bearing capacity of soil is weak, making it susceptible to external forces and deformation.

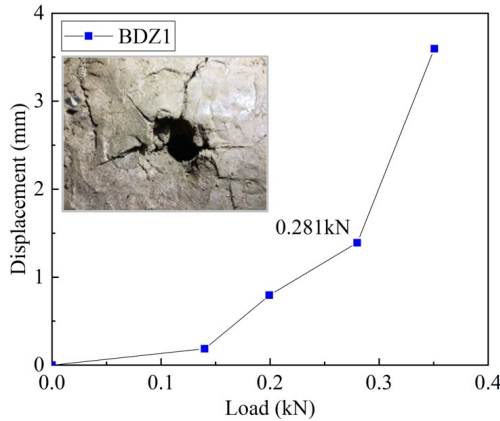


Fig. 4. Load displacement curve of BDZ1

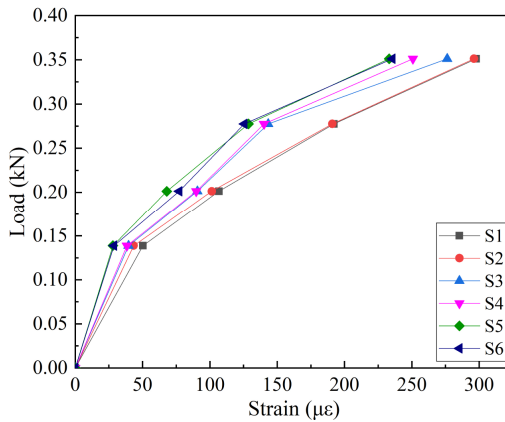


Fig. 5. Load-strain curve of BDZ1

The load-strain development at different parts of the pile body is shown in Fig. 5. The contact area between BDZ1 and the soil is small, and the strain shows a nonlinear growth characteristic. In addition, the strains near the pile top (i.e., S1, S2) are larger and develop faster. In comparison, the strains on the pile side with a greater burial depth are smaller (i.e., S4, S5) and develop slower. The reason is that when the pile top is subjected to uplift load, this load first acts directly on the soil near the pile top and the pile. The pile top is the direct load point, and the stress in this area will be relatively concentrated, resulting in a larger strain. When the load is transmitted downward from the pile top, it will gradually disperse and attenuate due to the pile body and soil interaction. As the burial depth increases, the frictional resistance of the pile side gradually

increases and effectively resists the uplift load. The increased frictional resistance limits the displacement of the lower part of the pile body, thereby reducing the strain at S5 and S6. Therefore, as the burial depth increases, the pile body strain decreases.

3.2 BDZ2

At the initial loading stage, the displacement and load of the BDZ2 specimen are approximately linearly related, as shown in Fig. 6. When the uplift load reaches a certain value, the corresponding uplift displacement increases rapidly. The uplift bearing capacity of BDZ2 is determined by the test to be 0.723kN, and the uplift displacement is 3.86mm. When the uplift load on the BDZ2 specimen reaches 0.992 kN, the pile is pulled out, so the loading is stopped. Compared with BDZ1, the uplift load of BDZ2 is larger. The reason is that as the pile length increases, the contact area between the pile and the surrounding soil also increases accordingly. When the pile is subjected to uplift force, the pile body can more effectively disperse and transfer the load to the surrounding soil, thereby improving the uplift capacity of the pile body. Therefore, the range of soil cracks around BDZ2 is significantly smaller than that of BDZ1.

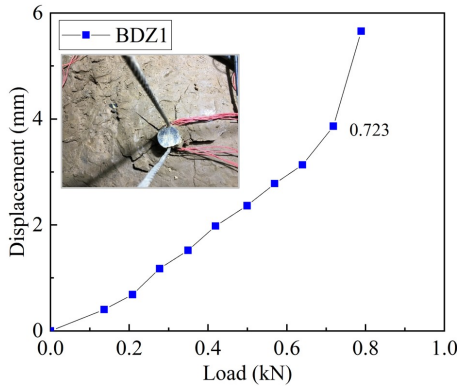


Fig. 6. Load displacement curve of BDZ2

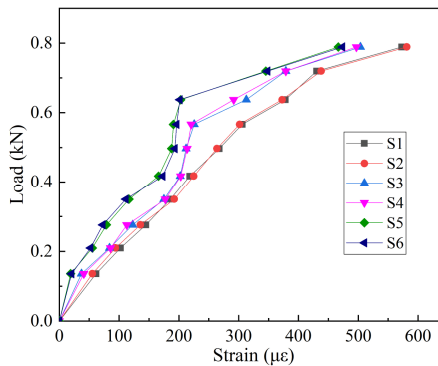


Fig. 7. Load-strain curve of BDZ2

The load-strain development at different locations of BDZ2 is shown in Fig. 7. In the initial loading stage, the pile and its surrounding soil are mainly in the elastic deformation stage, and the strain development is linear. As the load increases, the pile and its surrounding soil enter the elastic-plastic deformation stage. Eventually, the relationship between strain and load is no longer linear. Similar to BDZ1, the strain of the pile body close to the surface develops faster, and the strain of the pile body with a greater burial depth is smaller.

3.3 BDZ3

The load-displacement of specimens BDZ3 and BDZ2 have similar development trends. The displacement and load are approximately linear in the initial loading period. When the uplift load reaches a certain value, the displacement increases rapidly. The Load-displacement curve of BDZ3 is shown in Fig. 8. The test determines the uplift capacity to be 0.824 kN, and the uplift displacement is 8.08 mm. In this test, when the load reaches 1.33 kN, the pile is pulled out, and the loading is stopped. Compared with BDZ1 and BDZ2, the development of soil cracks in BDZ3 is not significant. This is because the friction area between the pile and the soil of BDZ3 is larger, and the soil is subjected to a more uniform force, resulting in a slow development of cracks.

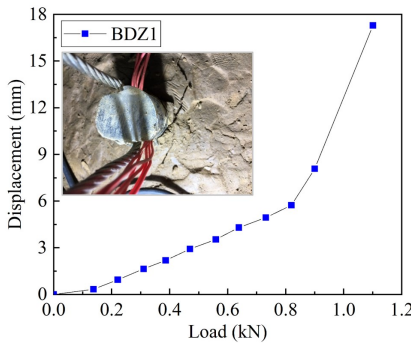


Fig. 8. Load displacement curve of BDZ3

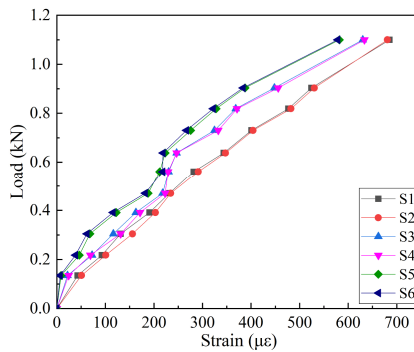


Fig. 9. Load-strain curve of BDZ3

The load-strain development at different parts of the pile body of the BDZ3 specimen is shown in Fig. 9. Obviously, the load-strain of the specimen shows a linear development trend during the loading process, which further illustrates that the soil is subjected to uniform stress. Finally, the model pile is pulled out because the load overcomes the friction between the pile and the soil.

3.4 Discussion of Test Results

In general, the uplift capacity of the pile increases with the increase of the slenderness ratio. Under the same uplift force, the pile with a slenderness ratio of 15 has the smallest uplift displacement and the strongest ability to resist deformation. The following conclusions can be drawn: the ultimate uplift capacity of a short pile foundation on a clay foundation is positively correlated with the slenderness ratio of the pile, and increasing the slenderness ratio can effectively enhance the uplift capacity of the pile. Therefore, in the design and construction of short pile foundations of transmission towers on clay foundations, key information such as the thickness of the clay layer, soil conditions, and groundwater level of the foundation need to be considered. In special cases such as clay, even though the pile length may be shorter, special consideration needs to be given to the pile's slenderness ratio to ensure the pile's stability and bearing capacity.

4 Theoretical Calculation of Uplift Capacity of Pile Foundation

4.1 Uplift Capacity

The ultimate uplift capacity of a single pile should be determined through static load tests. During the preliminary design, the standard value of the ultimate uplift capacity of a single pile is usually calculated based on an empirical formula, i.e., Eq. (1) [1].

$$P_{ut} = \sum_{i=1}^n \alpha_i \gamma_i U_i L_i q_{si} \quad (1)$$

where γ_i is the secondary grouting anti-pull adjustment coefficient, which is taken as 1.2 for the soil layer undergoing secondary grouting and take as 1.0 for soil layers that have not undergone secondary grouting. L_i is the thickness of the i -th layer of soil. U_i is the circumference of the pile. q_{si} is the standard value of the ultimate lateral resistance of the layer i -th of soil. α_i is the ultimate lateral friction resistance and uplift reduction coefficient of the layer i -th of soil. The value ranges from 0.70 to 0.80 for clay.

4.2 Discussion on Calculation Methods

The pull-out bearing capacities obtained by calculation and testing are shown in Table 2. It can be found that the calculated value is more conservative than the test value, and the error between the test value and the calculated value becomes larger as the pile

slenderness ratio increases. This is because the calculation formula for the uplift capacity in the specification is derived based on the shear failure mode of the uplift pile along the contact surface. However, the lower sidewall interface of the pile is shear-damaged in the test. At the same time, an oblique fracture surface is formed in the soil at a local depth in the upper part. Part of the soil in the conical area of the fracture surface adheres to the pile, presenting a composite shear failure mode, and the deadweight of this part of the soil cannot be ignored. Therefore, the standard formula for calculating the uplift capacity of short piles on clay foundations is conservative. In practice, the formula can be amplified based on the slenderness ratio of the short pile.

Table 2. Comparison between the test and calculated values

Specimens	F_t (kN)	F_c (kN)	Error (%)
BDZ1	0.281	0.269	4.5
BDZ2	0.723	0.678	6.7
BDZ2	0.824	0.750	9.9

Note: Error = $(F_t - F_c) / F_c \times 100\%$

5 Conclusion

A model test is carried out in this paper to study the uplift capacity and influencing factors of short pile foundation on clay foundation, and the following conclusions can be drawn:

(1) The uplift displacement at the initial loading stage is linearly related to the load. When the load reaches the ultimate uplift capacity, the specimen will fail quickly due to the pile being pulled out.

(2) The short pile showed a composite shear failure mode, with cracks forming in the soil around the pile. The conical soil in the upper oblique fracture surface adhered to the pile, thus affecting the uplift capacity of the short pile.

(3) The ultimate uplift capacity of short pile foundation on clay foundation positively correlates with the pile slenderness ratio. Increasing the pile slenderness ratio can effectively enhance the uplift resistance of the pile.

(4) The theoretical calculation value of the short pile foundation is relatively conservative. It can be appropriately enlarged based on the slenderness ratio of the specimen.

(5) In the design and construction of short pile foundations for transmission towers on clay foundations, even though the pile length may be shorter, special consideration needs to be given to the pile's slenderness ratio to ensure the pile's stability and bearing capacity.

Acknowledgments

The research work was supported by State Grid Jiangsu Economic Research Institute's 2024 Science and Technology Service Project

References

1. DL/T5486–2020. Technical specification for the design of steel supporting structures of overhead transmission line. National Energy Administration, Beijing, China; 2020.
2. Pan L, Chong J. Analytical method for laterally loaded short piles near clay slopes considering the soil-pile-slope surface deformation mechanism [J]. *Ocean Engineering*, 2024, 296: 117036. <https://doi.org/10.1016/j.oceaneng.2024.117036>
3. Richard C. S., Visar F., Behzad F., et al. A novel short pile foundation system bonded to highly cemented layers for settlement control [J]. *Canadian Geotechnical Journal*, 2023, 9(15): 1332-1351. <https://doi.org/10.1139/cgj-2020-0710>
4. Maosong H., He C., Zhenhao S., et al. Multi-directional T-EMSD-based p-y model for recent loading history effects on lateral response of short pile and caisson in undrained clays [J]. *Ocean Engineering*, 2022, 267(1): 113279. <https://doi.org/10.1016/j.oceaneng.2022.113279>
5. Zhang X, Zhang X, Xu C, et al. The calculation method of vertical bearing capacity of pile foundation considering cyclic weakening effect of soft clay [J]. *Computers and Geotechnics*, 2024, 172:106422. <https://doi.org/10.1016/j.compgeo.2024.106422>
6. Vaidas Martinkus. Experimental Investigation of Stress Distribution of Vertically Loaded Short Displacement Pile in Cohesion-less Soil [J]. *Procedia Engineering*, 2013, 57: 754-761. <https://doi.org/10.1016/j.proeng.2013.04.095>
7. Xu, CJ, Xu, YL, Sun, HL. Application of long-short pile retaining system in braced excavation [J]. *International journal of civil engineering*, 2015, 13: 81-89. <https://webofscience.clarivate.cn/wos/alldb/full-record/WOS:000365052500001>
8. Murali M, Grajales-Saavedra F J, Beemer R D, et al. Capacity of short piles and caissons in soft clay from geotechnical centrifuge tests[J]. *Journal of Geotechnical and Geoenvironmental Engineering*, 2019, 145(10): 04019079. [https://doi.org/10.1061/\(ASCE\)GT.1943-5606.0002091](https://doi.org/10.1061/(ASCE)GT.1943-5606.0002091)
9. DAs B M. Model tests for uplift capacity of foundations in clay[J]. *Soils and Foundations*, 1978, 18(2): 17-24. https://doi.org/10.3208/sandf1972.18.2_17
10. Gu, K.Y., Tran, N.X., Han, J.M., et al. Centrifuge study on the uplift behavior of spread foundation for transmission tower in sand [J]. *Canadian Geotechnical Journal*, 2024, 61(7):1418-1432. DOI:10.1139/cgj-2023-0065
11. Nguyen, D.K., Nguyen, T.P., Keawsawasvong, S., et al. A Vertical uplift capacity of circular anchors in clay by considering anisotropy and non-homogeneity [J]. *Transportation Infrastructure Geotechnology*, 2022, 9: 653-672. <https://link.springer.com/article/10.1007/s40515-021-00191-6>
12. BRAJA M. DAS. A procedure for estimation of ultimate uplift capacity of foundations in clay [J]. *Soils and foundations*, 1982, 20(1):77-82. <https://doi.org/10.3208/sandf1972.20.77>
13. Dash B K, Pise P J. Effect of compressive load on uplift capacity of model piles[J]. *Journal of Geotechnical and Geoenvironmental Engineering*, 2003, 129(11): 987-992. [https://doi.org/10.1061/\(ASCE\)1090-0241\(2003\)129:11\(987\)](https://doi.org/10.1061/(ASCE)1090-0241(2003)129:11(987))
14. Houslyby G T, Martin C M. Undrained bearing capacity factors for conical footings on clay[J]. *Géotechnique*, 2003, 53(5): 513-520. <https://doi.org/10.1680/geot.2003.53.5.513>
15. Reddy A S, Rao K N V. Bearing capacity of strip footing on anisotropic and nonhomogeneous clays[J]. *Soils and Foundations*, 1981, 21(1): 1-6. <https://doi.org/10.3208/sandf1972.21.1>
16. Wang, Y., Yang, Y., Yang, H., et al. Micro-macro analysis of the uplift behavior of the suction anchor in clay based on the CFD-DEM coupling model [J]. *Computers and Geotechnics*, 2024, 174: 106624. DOI:10.1016/j.compgeo.2024.106624

17. Zhang Y, Andersen K H, Tedesco G. Ultimate bearing capacity of laterally loaded piles in clay—Some practical considerations[J]. *Marine Structures*, 2016, 50: 260-275. <https://doi.org/10.1016/j.marstruc.2016.09.002>
18. Zhuang, D., Guo, W., Sun, L., et al. Effect of strain rate on triaxial extension behavior of silty clay [J]. *Marine Georesources & Geotechnology*, 2023, 41(4): 366-375. DOI:10.1080/1064119X.2022.2042630
19. Li X, Gaudin C, Tian Y, et al. Effects of preloading and consolidation on the uplift capacity of skirted foundations[J]. *Géotechnique*, 2015, 65(12): 1010-1022. <https://doi.org/10.1680/jgeot.15.P.026>
20. Zografou D, Gourvenec S, O'Loughlin C. Vertical cyclic loading response of shallow skirted foundation in soft normally consolidated clay[J]. *Canadian Geotechnical Journal*, 2019, 56(4): 473-483. <https://doi.org/10.1139/cgj-2018-0179>
21. Keawsawasvong, S., Yoang, S., Ukritchon, B. et al. Lower bound analysis of rectangular footings with interface adhesion factors on nonhomogeneous clays. [J]. *Computers and Geotechnics*, 2022, 147: 104787. DOI:10.1016/j.compgeo.2022.104787

Open Access This chapter is licensed under the terms of the Creative Commons Attribution-NonCommercial 4.0 International License (<http://creativecommons.org/licenses/by-nc/4.0/>), which permits any noncommercial use, sharing, adaptation, distribution and reproduction in any medium or format, as long as you give appropriate credit to the original author(s) and the source, provide a link to the Creative Commons license and indicate if changes were made.

The images or other third party material in this chapter are included in the chapter's Creative Commons license, unless indicated otherwise in a credit line to the material. If material is not included in the chapter's Creative Commons license and your intended use is not permitted by statutory regulation or exceeds the permitted use, you will need to obtain permission directly from the copyright holder.

